

# Multiplexing System for Automated Characterization of a Capacitive Field-Effect Sensor Array

Tobias Karschuck, Stefan Schmidt, Stefan Achtsnicht, Arshak Poghossian, Patrick Wagner, and Michael Josef Schöning\*

In comparison to single-analyte devices, multiplexed systems for a multianalyte detection offer a reduced assay time and sample volume, low cost, and high throughput. Herein, a multiplexing platform for an automated quasi-simultaneous characterization of multiple (up to 16) capacitive field-effect sensors by the capacitive–voltage ( $C-V$ ) and the constant-capacitance (ConCap) mode is presented. The sensors are mounted in a newly designed multicell arrangement with one common reference electrode and are electrically connected to the impedance analyzer via the base station. A Python script for the automated characterization of the sensors executes the user-defined measurement protocol. The developed multiplexing system is tested for pH measurements and the label-free detection of ligand-stabilized, charged gold nanoparticles.

## 1. Introduction

The electrolyte–insulator–semiconductor capacitor (EISCAP) represents the simplest biochemically sensitive field-effect device. Similar to other types of field-effect biochemical sensors, EISCAPs are very sensitive to any kind of potential (or charge) changes induced via biochemical reactions at or nearby the

gate-insulator/electrolyte interface. Due to the simple structure and easy fabrication, the EISCAP platform has been widely applied for designing a large variety of biochemical sensors capable of concentration measurements of ions<sup>[1–3]</sup> and metabolites,<sup>[4–9]</sup> as well as for the label-free detection of charged biomolecules,<sup>[10–15]</sup> virus particles,<sup>[16–18]</sup> carbon nanotubes,<sup>[19]</sup> and nanoparticle/molecule hybrids<sup>[20–22]</sup> by their intrinsic charge. Moreover, EISCAPs have been applied for the creation of biomolecular logic gates.<sup>[23,24]</sup> For recent progress in the field of EISCAP-based chemo- and biosensors, see the recent review article of Poghossian and Schöning.<sup>[25]</sup>


Typically, the electrochemical characterization of EISCAPs is performed with a single sensor mounted in an appropriate measurement cell. In contrast, in the last years, multiplexed (quasi) simultaneous assaying of multianalytes utilizing an array of single or on-chip integrated field-effect devices (FEDs) have received enormous attention.<sup>[26]</sup> In comparison to single-analyte detection devices, multianalyte detection systems may offer a reduced assay time and sample volume, low costs, and high throughput. Moreover, the multiplexed detection of multianalytes (e.g., a panel of clinically relevant cancer or cardiac biomarkers) will provide a more reliable diagnosis of diseases. While arrays of single or on-chip integrated transistor-type (e.g., ion-sensitive field-effect transistors,<sup>[27–30]</sup> silicon-nanowire transistors,<sup>[31–34]</sup> graphene-based transistors)<sup>[35]</sup> and light-addressable FEDs<sup>[36–38]</sup> have extensively been studied for multiparameter/multianalyte detection, the multiplexed assaying with EISCAPs still remains a challenging task. Several on-chip fabricated EISCAP sensors will stay interconnected through a common Si substrate that may result in undesired cross-talk between the sensors. Only a few studies, related to an array of on-chip, integrated EISCAPs for simultaneous or multiplexed detection, have been reported so far.<sup>[39–42]</sup> These developments have demonstrated the possibility to realize an array of on-chip integrated, individually electrically addressable EISCAPs. However, they resulted either in a loss of the EISCAPs' main advantages (simple layout, easy and cost-efficient preparation) or they required a separate electrolyte reservoir with an on-chip integrated pseudo-reference thin-film electrode for each individual EISCAP in the array (including a large drift and instable sensor signal). Another approach for a multiplexed array of single EISCAPs was proposed in the study of Schusser et al.,<sup>[43]</sup> where each individual sensor required its own separate measurement cell with additional reference electrode.

T. Karschuck, S. Schmidt, S. Achtsnicht, M. J. Schöning  
Institute of Nano- and Biotechnologies  
FH Aachen  
52428 Jülich, Germany  
E-mail: schoening@fh-aachen.de

T. Karschuck, P. Wagner  
Laboratory for Soft Matter and Biophysics  
KU Leuven  
3001 Leuven, Belgium

A. Poghossian  
MicroNanoBio  
40479 Düsseldorf, Germany

M. J. Schöning  
Institute of Biological Information Processing (IBI-3)  
Forschungszentrum Jülich  
52425 Jülich, Germany

 The ORCID identification number(s) for the author(s) of this article can be found under <https://doi.org/10.1002/pssa.202300265>.

© 2023 The Authors. *physica status solidi (a)* applications and materials science published by Wiley-VCH GmbH. This is an open access article under the terms of the Creative Commons Attribution-NonCommercial License, which permits use, distribution and reproduction in any medium, provided the original work is properly cited and is not used for commercial purposes.

DOI: 10.1002/pssa.202300265

In this work, we present a multiplexing system for the characterization of multiple (up to 16) individually addressable EISCAPs mounted in a multicell having only one RE. The system allows quasi-simultaneous readout of multiple EISCAP signals in convenient capacitance–voltage ( $C-V$ ) and constant-capacitance (ConCap) modes by simple multiplexing of sensors using a custom-developed software in a Python script. The multiplexing system with the newly developed multicell was tested and validated for pH measurements and the label-free detection of ligand-stabilized, charged gold nanoparticles (AuNP) using  $p-Si-SiO_2-Ta_2O_5$  and  $p-Si-SiO_2$  EISCAPs, respectively.

## 2. Multicell Arrangement

For the EISCAP characterization, we used the electrochemical workstation Zahner IM6ex (Zahner Elektrik, Germany) with integrated relay-multiplexer (RMux), which enables multiplexing of up to 16 sensors. Therefore, the multicell was designed for maximum 16 EISCAPs. Design requirements for the multicell arrangement for the multiplexed characterization of EISCAPs and the multiplexed system have recently been formulated in Karschuck et al.<sup>[44]</sup> and are briefly listed below: 1) Easy, interchangeable, and nondestructive installation and dismantling of the EISCAPs; one RE for all EISCAPs in the array to ensure comparability and cost-effectiveness; 2) The designed multicell platform should allow the immobilization/deposition of different chemical/biological recognition elements (receptors), making the system highly versatile for many applications; 3) Easy integration of the multicell arrangement with the impedance analyzer; and 4) Fully automated multiplexed detection and characterization with minimal user training.

The 3D design of the multicell arrangement with the multicell for 16 sensors and the base station is shown in **Figure 1a**. To ensure a waterproof finish, the top part of the multicell was made from a solid block of polymethyl methacrylate. Fluidic pathways

from the center of the multicell to the individual sensor reservoirs were approximately the same ( $\approx 48$  mm). O-rings are used as watertight seal between the sensors and the top part of the multicell. The buffer volume in the measurement cell is about 20 mL. Each sensor reservoir can hold up to a maximum sample volume of 0.4 mL.

The design of the multicell offers an easy mounting in the base station and features a printed circuit board (PCB) equipped with spring-loaded contact pins, 44-pin D-Subminiature (D-Sub) port for the electrical connection to the RMux card, and a RE connector (see **Figure 1a**). The individual EISCAP sensors mounted into the multicell are connected via spring-loaded contact pins on the PCB, thus, making the multicell easy exchangeable.

**Figure 1b** shows the position of sensors in the multicell (top) and a photo of the multicell inside the base station (bottom). The base station with the multicell is closed with the cover plate, having a centered holder for mounting of the RE (see **Figure 1b**). In some configurations, the cover plate may have additional holders for a control pH electrode, electrolyte-conductivity probe, and/or temperature sensor.

In contrast to complicated on-chip integrated EISCAP arrays described in the previous studies,<sup>[39–41]</sup> we use in this work an array of single EISCAP sensors, which are easy and cost-efficient in preparation. In contrast to the study of Dastidar et al.<sup>[41]</sup> and Schusser et al.,<sup>[43]</sup> our multicell requires only one conventional reference electrode to ensure comparability of the measurement results and cost-effectiveness. In addition, the presented multicell design enables the characterization of up to 16 sensors, practically excluding cross-talk effects between the individual sensors.

## 3. Results and Discussion

### 3.1. Multiplexed pH Measurements with 16 EISCAPs

Before starting the experiments on multiplexed pH measurements, the  $Ta_2O_5$ -gate EISCAPs mounted in the multicell were

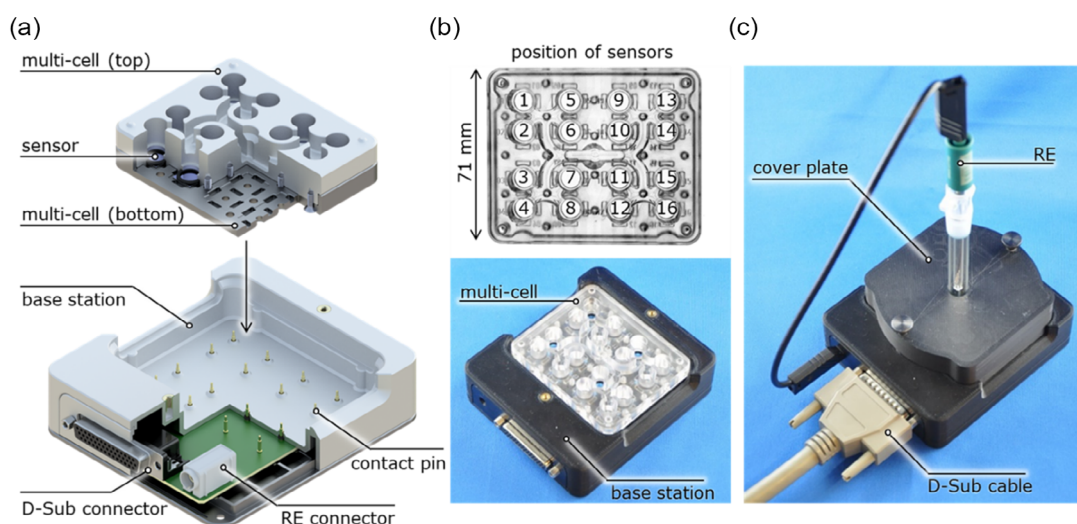


**Figure 1.** a) Exploded view of the multicell arrangement (top) and the base station (bottom). The D-Sub connector serves as interface between the base station and the impedance analyzer. The RE can be directly connected to the base station. The sensors are electrically connected via spring-loaded contact pins. b) Position of sensors in the multicell (top) and photo of the multicell inside the base station (bottom). c) Photo of the fully assembled multiplexing system with connected RE and D-Sub cable.

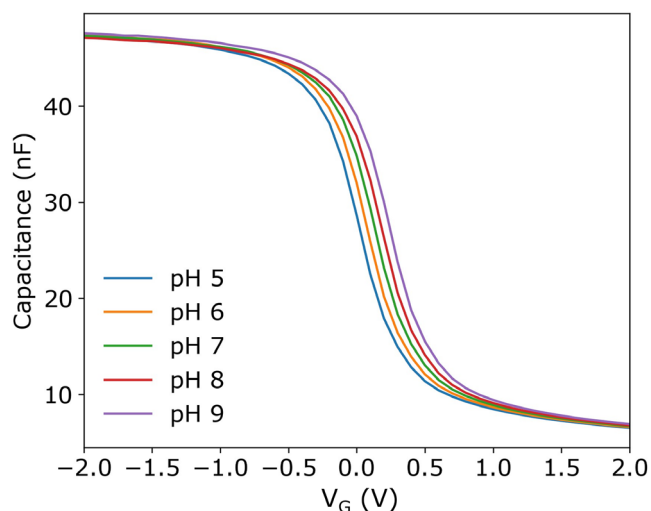


**Figure 2.**  $C$ - $V$  curves of the Sensor-1 recorded in Titrisol buffer solutions of different pH values between pH 5 and pH 9 using the multicell arrangement.

conditioned at room temperature overnight in pH 7 buffer solution (Titrisol, Merck, Germany). The EISCAP sensors were characterized in terms of pH sensitivity in Titrisol buffer solutions of different pH values between pH 5 and pH 9. **Figure 2** shows exemplary collected high-frequency  $C$ - $V$  curves of Sensor-1 with characteristic regions of accumulation ( $V_G < -1.5$  V), depletion ( $-0.5 < V_G < 0.5$  V), and inversion ( $V_G > 1.5$  V). As expected, with the increasing pH value of the buffer from pH 5 to pH 9, the  $C$ - $V$  curves were shifted along the voltage axis in the direction of more positive voltages values, which corresponds to a more negatively charged gate surface.

The generally accepted model describing the mechanism of pH sensitivity of FEDs with oxide gate insulators (here,  $\text{Ta}_2\text{O}_5$ ) is the site-binding model.<sup>[45,46]</sup> The surface of  $\text{Ta}_2\text{O}_5$  contains neutral amphoteric hydroxyl groups ( $\text{TaOH}$ ) which are either able to bind or release a proton ( $\text{H}^+$ ), resulting in protonated ( $\text{TaOH}_2^+$ ), or deprotonated ( $\text{TaO}^-$ ) groups.<sup>[25]</sup> Thus, the pH-dependent surface charge of the  $\text{Ta}_2\text{O}_5$  gate will modulate the space-charge capacitance in the Si and, finally, the total capacitance of the EISCAP. For instance, in case of a p-type Si-based EISCAP used in this study, an increase of the pH value will lead to a decrease of the width of the depletion layer. As a consequence, the total capacitance of the sensor will increase, resulting in a shift of the  $C$ - $V$  curve toward more positive gate voltages. Conversely, a pH decrease will increase the width of the depletion layer, yielding a decrease of the total capacitance of the sensor. This will result in a shift of the  $C$ - $V$  curves toward more negative (or less positive) gate voltages.

The working points, i.e., the constant-capacitance value ( $C_{wp}$ ) for recording the ConCap signal of individual sensors were determined from the  $C$ - $V$  curves registered in pH 7 buffer and are listed in **Table 1**. The EISCAP chips diced from the same wafer show high reproducibility of  $C_{wp}$ .

The results of the normalized ConCap signals of 16 EISCAPs in buffer solutions with different pH values are presented in **Figure 3**. The ConCap signals of all EISCAPs measured in the loop of pH 7-6-5-6-7-8-9-8-7 show identical behavior with a clear pH dependence. After each pH measurement, the

**Table 1.** Working points and pH sensitivities of sensor-1 to sensor-16.

Sensor	$C_{wp}$ [nF]	pH sensitivity [ $\text{mV pH}^{-1}$ ]	Sensor	$C_{wp}$ [nF]	pH sensitivity [ $\text{mV pH}^{-1}$ ]
1	27.7	55	9	28.6	57
2	26.8	57	10	26.7	56
3	27.6	54	11	27.3	57
4	28.2	56	12	27.5	57
5	28.8	58	13	29.6	58
6	29.8	56	14	27.3	57
7	28.1	54	15	29.7	56
8	27.4	57	16	27.3	53

Python script automatically plots a measurement graph, summarizing the results of the particular measurement, which gives an additional quality control for the operator. In this way, potential outliers due to improperly working sensors can be spotted.

The calibration curves of the EISCAPs evaluated from the respective normalized ConCap responses (in **Figure 3**) are depicted in **Figure 4**. The pH sensitivity of each EISCAP, determined from the respective calibration curve, is given in **Table 1**. The average pH sensitivity of 16  $\text{Ta}_2\text{O}_5$ -gate EISCAP sensors was  $56.4 \pm 1.5 \text{ mV pH}^{-1}$ , which is in good agreement with the pH sensitivity of  $\text{Ta}_2\text{O}_5$  layers prepared by atomic layer deposition,<sup>[1,47]</sup> electron-beam evaporation<sup>[48]</sup> and thermal oxidation of sputtered Ta films.<sup>[49,50]</sup>

### 3.2. Multiplexed Label-Free Detection of Ligand-Stabilized Charged AuNPs

In addition to pH measurements, we used aminooctanethiol (AOT)-stabilized AuNPs (AOT-AuNPs) as a model system to examine the capability of a  $\text{SiO}_2$ -gate EISCAP array to detect charged nanoparticles. The AOT-AuNPs with a core diameter of  $17.2 \pm 2.2 \text{ nm}$  were prepared from negatively charged citrate-covered AuNP (Ct-AuNP) via the ligand-exchange reaction from citrate to aminooctanethiol.<sup>[51]</sup> The Ct-AuNPs were synthesized by the well-known Turkevich method using the tetrachloroauric acid ( $\text{HAuCl}_4$ ,  $c = 375 \mu\text{M}$ ) reduction reaction.<sup>[52,53]</sup> Measurements of the zeta potential of Ct-AuNPs ( $-45 \pm 2 \text{ mV}$ ) and AOT-AuNPs ( $+21 \pm 1 \text{ mV}$ ) by electrophoretic light scattering using the Litesizer 500 (Anton Paar, Germany) have verified the successful ligand exchange from negatively charged citrate (due to the carboxylic acid groups of the citrate molecules) to positively-charged AOT (due to the ammonium groups).<sup>[22]</sup> Details of the Ct-AuNPs and AOT-AuNPs preparation process steps can be found in the previous studies.<sup>[21,51]</sup>

Before the AOT-AuNP immobilization experiments, all 16  $\text{SiO}_2$ -gate EISCAPs in the multicell were conditioned in the measurement buffer (0.33 mM PBS, pH 4) overnight. After recording the multiplexed ConCap responses of the 16 bare EISCAPs in the measurement buffer, they were split into two groups (G1 and G2) of eight EISCAPs each. For the AOT-AuNP immobilization, the surface of EISCAPs in group G1 was exposed to the immobilization buffer ( $1 \times \text{PBS}$ , pH 3) spiked with 5.5 nM AOT-AuNPs for 2 h. At the same time, for comparison, the surface of

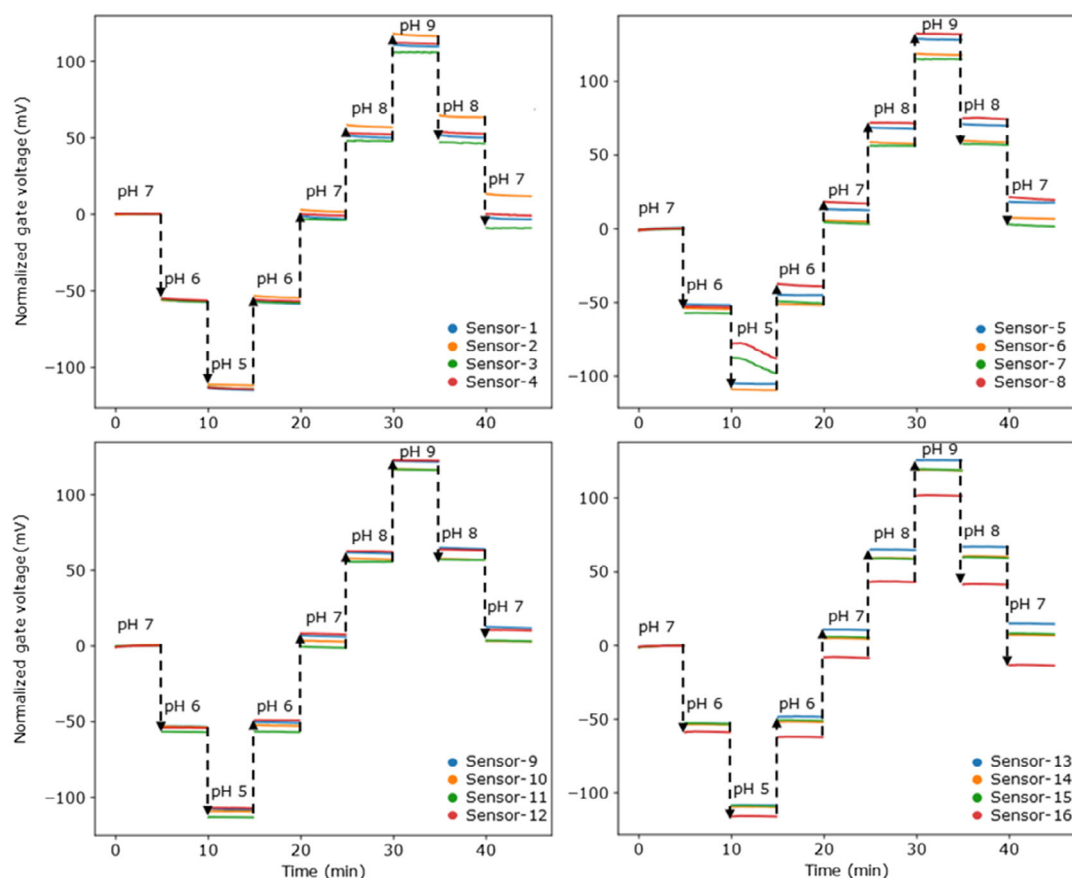


**Figure 3.** Normalized ConCap signals of 16 EISCAPs measured in the loop of pH 7-6-5-6-7-8-9-8-7 using the multicell arrangement. The gate voltages of all sensors were normalized to the first measurement at pH 7.

EISCAPs in reference group G2 was exposed to the same buffer solution but without AOT-AuNPs for 2 h. Afterward, the surface of all EISCAP chips was rinsed three times with the measurement buffer, followed by the electrochemical characterization in the measurement buffer.

**Figure 5a** depicts normalized ConCap responses of EISCAPs before and after exposure to the immobilization buffer with and without AOT-AuNPs. As expected, the normalized ConCap signals of the EISCAPs modified with positively charged AOT-AuNPs (group G1) shift in the direction of negative voltages by about  $-24$  to  $-28$  mV. The direction of the observed voltage shifts corresponds to a more positively charged gate surface.<sup>[25,54]</sup> To keep the EISCAP capacitance at a constant value in the ConCap mode, the feedback control provides a more negative voltage on the gate for compensation of the positive charge of the immobilized AOT-AuNPs.

In contrast, the ConCap signal shifts of unmodified EISCAPs (group G2) amount to approximately  $-5$  to  $-9$  mV and can be attributed to the drift of the SiO<sub>2</sub>-gate EISCAPs associated with the relatively slow chemical modification of the gate insulator surface as a result of exposure to the electrolyte<sup>[55]</sup> (here, immobilization buffer (pH 3) for 2 h). For instance, in previous experiments, drift values in the range from 8 mV per day<sup>[56]</sup> up to 4.8 – 19.6 mV per hour<sup>[57]</sup> in pH 7 buffer were reported for SiO<sub>2</sub>-gate EISCAPs. However, the ConCap signal changes induced by

the immobilization of AOT-AuNPs were much higher than those caused by the drift effect. By assuming similar drift values for G1 and G2, the net averaged differential ConCap signal shift (induced by the immobilized charged AOT-AuNPs) evaluated from **Figure 5a** is  $-18.4 \pm 1.1$  mV.

Finally, in separate experiments, the surface coverage of AOT-AuNPs on the EISCAP chips has been determined from scanning electron microscopy (SEM) images. The SEM images of the AOT-AuNP-modified EISCAP surface were taken with the JSM-7800F microscope (Jeol GmbH, Germany), where a representative image of the AOT-AuNP-modified EISCAP surface is shown in **Figure 5b**.

The average surface coverage of AOT-AuNPs calculated from SEM images using an ImageJ macro<sup>[58]</sup> was  $9.5\% \pm 2.3\%$ . Thus, the EISCAPs integrated with the newly developed multicell were able for a label-free multiplexed detection of even low surface coverages of charged AOT-AuNPs. Other benefits of the multicell arrangements are the possibility of differential measurements and a statistical analysis of multiple EISCAP signals after only one experiment.

## 4. Conclusion

The design of a new multicell arrangement allows easy, interchangeable, and nondestructive installation and dismantling

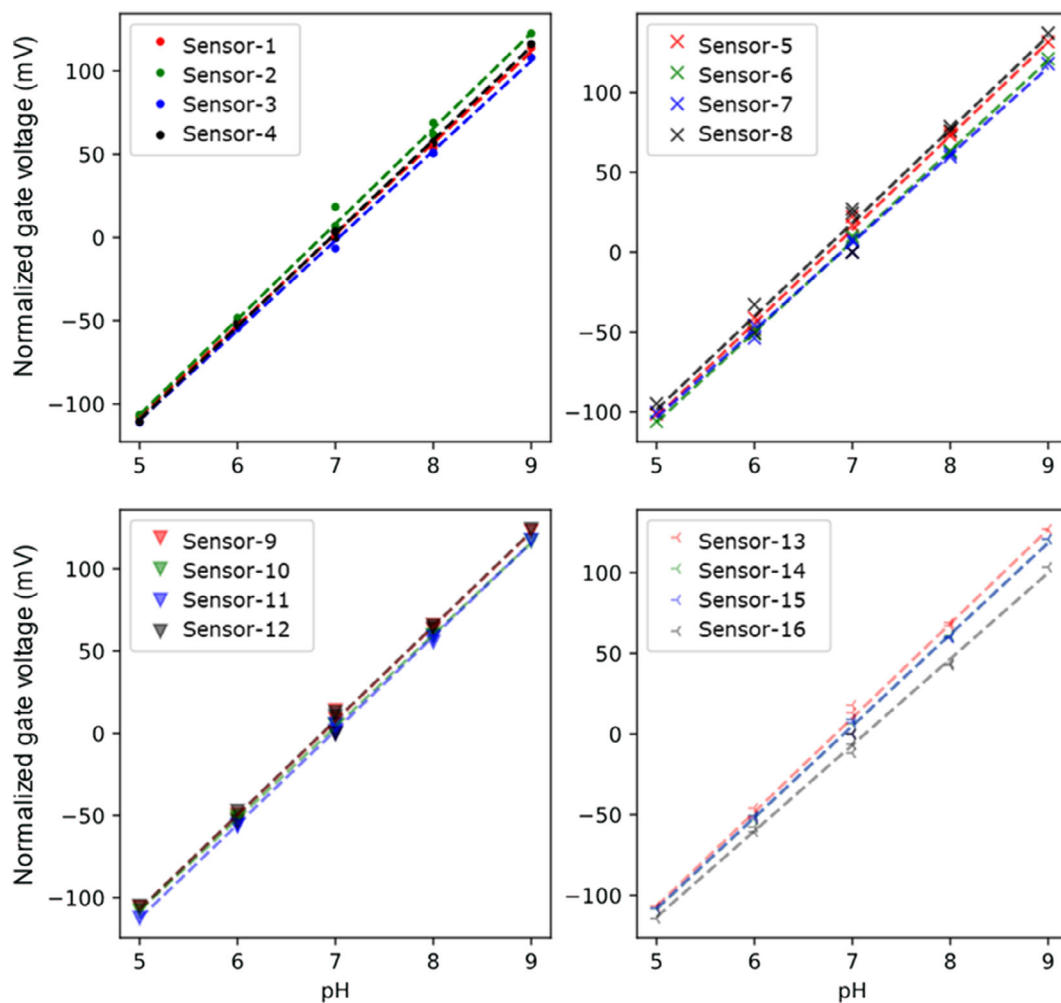


**Figure 4.** Calibration curves of Sensor-1 to Sensor-16 evaluated from the normalized ConCap signals in Figure 3.

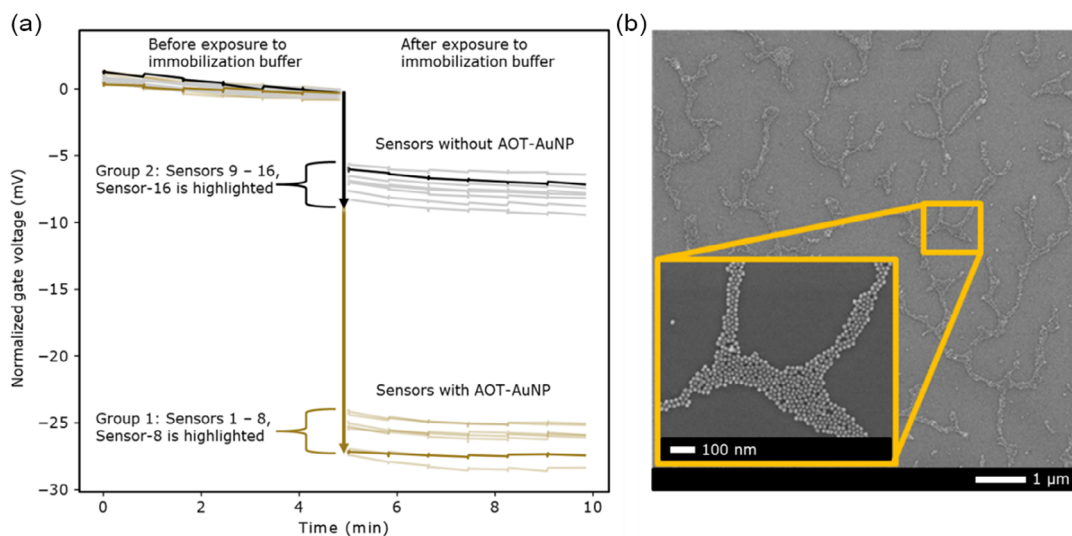


**Figure 5.** a) Normalized ConCap responses of  $\text{SiO}_2$ -gate EISCAPs before and after exposure to the immobilization buffer with (group 1) and without (group 2) AOT-AuNPs with Sensor-8 and Sensor-16 exemplary highlighted. b) Representative SEM image of the AOT-AuNP-modified EISCAP surface.

of EISCAPs with one reference electrode shared by all sensors. The comfortable integration of the multicell system with the impedance analyzer enables a fully automated, multiplexed measurement and characterization of EISCAPs (with minimal user training required).

The multiplexed system has been successfully tested regarding pH characterizations of 16 p-Si-SiO<sub>2</sub>-Ta<sub>2</sub>O<sub>5</sub> EISCAP sensors. The determined average pH sensitivity of 56.4 ± 1.5 mV pH<sup>-1</sup> is in good agreement with literature data for the pH sensitivity of Ta<sub>2</sub>O<sub>5</sub> layers.<sup>[1,47–50]</sup>

For the detection of diverse analytes, the mitigation of interfering influences, such as temperature, drift, or pH variations in the measurement buffer, is desirable. This can be achieved by incorporating a differential measurement setup. As an example, AOT-AuNPs with a core diameter of 17.2 ± 2.2 nm were successfully immobilized on p-Si-SiO<sub>2</sub> EISCAPs mounted in the multicell. For an AOT-AuNP coverage of 9.5% ± 2.3% on the sensor surface, an averaged net differential ConCap signal of -18.4 ± 1.1 mV between EISCAPs with and EISCAPs without AOT-AuNPs was evaluated by assuming comparable drift behavior for the sensors.

The implementation of the multicell into a field-effect-based fluidic system<sup>[59]</sup> is prospectively planned as it would allow buffer exchanges without the need to remove the multicell from the base station.

## 5. Experimental Section

**Fabrication of EISCAP Sensors:** Two types of EISCAPs consisting of either Al-p-Si-SiO<sub>2</sub> or Al-p-Si-SiO<sub>2</sub>-Ta<sub>2</sub>O<sub>5</sub> structures were fabricated using a commercially available p-Si-SiO<sub>2</sub> wafer (with 30 nm SiO<sub>2</sub> prepared by dry thermal oxidation, Siebert Wafer, Germany). The SiO<sub>2</sub>-gate EISCAPs were applied in experiments on multiplexed detection of ligand-stabilized AuNPs. The Ta<sub>2</sub>O<sub>5</sub>-gate EISCAPs were used for multiplexed pH measurements, because Ta<sub>2</sub>O<sub>5</sub> belongs to the best pH-sensitive materials, exhibiting a nearly-Nernstian pH sensitivity, small drift and a low hysteresis.<sup>[1,25,27,49,60]</sup>

The fabrication process steps of EISCAPs were described previously (see e.g.,<sup>[7,17]</sup>). Briefly, the Ta<sub>2</sub>O<sub>5</sub> layer (60 nm) was prepared by electron-beam evaporation of a 30 nm tantalum layer and subsequent oxidation under oxygen atmosphere at 520 °C for 60 min. Then, the rear side of both p-Si-SiO<sub>2</sub> and p-Si-SiO<sub>2</sub>-Ta<sub>2</sub>O<sub>5</sub> wafers was etched by hydrofluoric acid (HF, 5%), and an aluminum layer (300 nm) was deposited on it as contact layer by electron-beam evaporation and annealed under nitrogen atmosphere at 400 °C for 10 min. Individual SiO<sub>2</sub>-gate and Ta<sub>2</sub>O<sub>5</sub>-gate EISCAP chips (10 mm × 10 mm) were diced from the respective wafer, and cleaned in an ultrasonic bath with acetone, isopropanol, ethanol, and deionized water for 3 min each.

**Electrochemical Characterization of EISCAP Sensors:** The 16 sensors were connected to the R-Mux multiplexer card of the electrochemical workstation Zahner IM6ex. The liquid-junction Ag/AgCl reference electrode (filled with 3M KCl, Metrohm, Filderstadt, Germany), which was mounted in the center of the multicell and immersed in the electrolyte, closed the electrical circuit for the selected channel of the multiplexer card. A Python script based on the GitHub repository of Zahner Elektrik, was used to automatically handle all stages of the measurements.<sup>[61]</sup>

The EISCAP represents a biochemically sensitive capacitor. In a simplified equivalent circuit model, the total capacitance of the EISCAP can be described as a series connection of the constant capacitance of the gate insulator (in this study, SiO<sub>2</sub> or SiO<sub>2</sub>-Ta<sub>2</sub>O<sub>5</sub>) and a variable capacitance of the space-charge region in the Si, which depends, among others, on the gate voltage ( $V_G$ ) and the potential at the insulator/electrolyte interface.<sup>[23]</sup> Convenient methods of electrochemical characterization of EISCAPs

include the C-V and ConCap modes (see e.g.,<sup>[25,62]</sup>). For the EISCAP characterization in the C-V mode, a sweeping direct-current gate voltage,  $V_G$  (between -2 and 2 V in 100 mV steps), and a small alternating-current voltage of 20 mV with a frequency of 120 Hz was applied between the RE and the rear-side contact of the selected EISCAP chip. The C-V curves recorded in buffer solution at different positions of the RE, e.g., in the center of the multicell on top of the different sensor chips, were identical (data not shown). Thus, by the measuring conditions used in this study, the distance between the EISCAP location and the position of the RE in the multicell arrangement has practically no impact on the measurement results.

After the C-V measurement, the operating point (i.e., the constant-capacitance value) for recording the ConCap signal was automatically set by a Python script within the linear range of the depletion region of the C-V curve, where the capacitance is more sensitive to potential changes (typically, at approximately 60% of the maximum capacitance registered in the accumulation region<sup>[23]</sup>; in this study, at  $V_G = -2$  V). In the ConCap mode, the surface potential changes (e.g., induced by the pH change or adsorption/binding of charged biomolecules/nanoparticles) are compensated by applying a gate voltage of opposite polarity, while keeping the total capacitance of the EISCAP constant. This allows a time-resolved monitoring of potential variations on the EISCAP gate surface. For multiplexed operation in the ConCap mode, each EISCAP was measured sequentially for 2 s, starting with Sensor-1 and continuing to Sensor-16. This cycle was repeated consecutively for a measurement time of usually 5–10 min. During the 2 s measurement period, three data points are collected. Furthermore, there is an approximate 48 s interval between the first measurement of a sensor and the subsequent measurement of the same sensor. All measurements were performed at room temperature in a dark Faraday cage to avoid the possible influence of ambient light and electromagnetic fields. The contact area of the gate surface with the solution was approximately 0.5 cm<sup>2</sup> for all EISCAPs mounted in the multicell.

## Acknowledgements

The authors would like to thank C. Kaulen, D. Rolka, S. Beging, and H. Iken for technical support and valuable discussions. Part of this work was supported by the Deutsche Forschungsgemeinschaft (DFG, German Research Foundation—445454801).

Open Access funding enabled and organized by Projekt DEAL.

## Conflict of Interest

The authors declare no conflict of interest.

## Data Availability Statement

The data that support the findings of this study are available from the corresponding author upon reasonable request.

## Keywords

capacitive field-effect sensor, gold nanoparticles, label-free detection, multicell, multiplexing, pH sensing

Received: April 4, 2023

Revised: June 2, 2023

Published online: September 6, 2023

[1] D. Molinnus, H. Iken, A. L. Johnen, B. Richstein, L. Hellmich, A. Poghossian, J. Knoch, M. J. Schöning, *Phys. Status Solidi A* **2022**, 219, 2100660.

[2] Y. Mourzina, T. Mai, A. Poghossian, Y. Ermolenko, T. Yoshinobu, Y. Vlasov, H. Iwasaki, M. J. Schöning, *Electrochim. Acta* **2003**, 48, 3333.

- [3] H. Cho, K. Kim, M. Meyyappan, C.-K. Baek, *Sens. Actuators, B* **2019**, 279, 183.
- [4] Y.-H. Lin, S.-H. Wang, M.-H. Wu, T.-M. Pan, C.-S. Lai, J.-D. Luo, C.-C. Chiou, *Biosens. Bioelectron.* **2013**, 43, 328.
- [5] C. F. Lin, C. H. Kao, C. Y. Lin, K. L. Chen, Y. H. Lin, *Nanomaterials* **2020**, 10, 583.
- [6] A. Poghossian, M. Jablonski, C. Koch, T. S. Bronder, D. Rolka, C. Wege, M. J. Schöning, *Biosens. Bioelectron.* **2018**, 110, 168.
- [7] M. Welden, A. Poghossian, F. Vahidpour, T. Wendlandt, M. Keusgen, W. Christina, M. J. Schöning, *Bioelectrochemistry* **2023**, 151, 108397.
- [8] W. Noura, H. Barhoumi, A. Maaref, N. Renault-Jaffrézic, M. Siadat, *J. Phys. Conf. Ser.* **2013**, 416, 12010.
- [9] A. Poghossian, M. Thust, P. Schroth, A. Steffen, H. Lüth, M. J. Schöning, *Sens. Mater.* **2001**, 13, 207.
- [10] J. Fritz, E. B. Cooper, S. Gaudet, P. K. Sorger, S. R. Manalis, *Proc. Natl. Acad. Sci. U. S. A* **2002**, 99, 14142.
- [11] T.-M. Pan, K.-Y. Chang, C.-W. Lin, S.-W. Tsai, M.-H. Wu, *J. Mater. Chem.* **2012**, 22, 1358.
- [12] T.-M. Pan, T.-W. Lin, C.-Y. Chen, *Anal. Chim. Acta* **2015**, 891, 304.
- [13] N. Kumar, S. Kumar, J. Kumar, S. Panda, *J. Electrochem. Soc.* **2017**, 164, B409.
- [14] R. Chand, D. Han, S. Neethirajan, Y.-S. Kim, *Sens. Actuators, B* **2017**, 248, 973.
- [15] M. Bahri, A. Baraket, N. Zine, M. Ben Ali, J. Bausells, A. Errachid, *Talanta* **2020**, 209, 120501.
- [16] A. Poghossian, M. Jablonski, D. Molinnus, C. Wege, M. J. Schöning, *Front. Plant. Sci.* **2020**, 11, 598103.
- [17] M. Jablonski, A. Poghossian, R. Severins, M. Keusgen, C. Wege, M. J. Schöning, *Micromachines* **2021**, 12, 57.
- [18] M. Jablonski, A. Poghossian, M. Keusgen, C. Wege, M. J. Schöning, *Anal. Bioanal. Chem.* **2021**, 413, 5669.
- [19] J. R. Siqueira, M. H. Abouzar, M. Bäcker, V. Zucolotto, A. Poghossian, O. N. Oliveira, M. J. Schöning, *Phys. Status Solidi A* **2009**, 206, 462.
- [20] A. Poghossian, M. Bäcker, D. Mayer, M. J. Schöning, *Nanoscale* **2015**, 7, 1023.
- [21] T. Karschuck, C. Kaulen, A. Poghossian, P. H. Wagner, M. J. Schöning, *Electrochem. Sci. Adv.* **2022**, 2, e2100179.
- [22] A. Poghossian, T. Karschuck, P. Wagner, M. J. Schöning, *Biosensors* **2022**, 12, 334.
- [23] A. Poghossian, K. Malzahn, M. H. Abouzar, P. Mehndiratta, E. Katz, M. J. Schöning, *Electrochim. Acta* **2011**, 56, 9661.
- [24] E. Katz, A. Poghossian, M. J. Schöning, *Anal. Bioanal. Chem.* **2017**, 409, 81.
- [25] A. Poghossian, M. J. Schöning, *Sensors* **2020**, 20, 5639.
- [26] B. Gil Rosa, O. E. Akingbade, X. Guo, L. Gonzalez-Macia, M. A. Crone, L. P. Cameron, P. Freemont, K.-L. Choy, F. Güder, E. Yeatman, D. J. Sharp, B. Li, *Biosens. Bioelectron.* **2022**, 203, 114050.
- [27] A. Poghossian, H. Lüth, J. Schultze, M. Schöning, *Electrochim. Acta* **2001**, 47, 243.
- [28] A. Poghossian, J. W. Schultze, M. J. Schöning, *Sens. Actuators, B* **2003**, 91, 83.
- [29] S. Cheng, S. Hideshima, S. Kuroiwa, T. Nakanishi, T. Osaka, *Sens. Actuators, B* **2015**, 212, 329.
- [30] K. Si, S. Cheng, S. Hideshima, S. Kuroiwa, T. Nakanishi, T. Osaka, *Sens. Mater.* **2018**, 833.
- [31] G.-J. Zhang, K. T. C. Chai, H. Z. H. Luo, J. M. Huang, I. G. K. Tay, A. E.-J. Lim, M. Je, *Biosens. Bioelectron.* **2012**, 35, 218.
- [32] J.-Y. Kim, J.-H. Ahn, D.-I. Moon, T. J. Park, S. Y. Lee, Y.-K. Choi, *Biosens. Bioelectron.* **2014**, 55, 162.
- [33] Y. Zhang, R. Chen, L. Xu, Y. Ning, S. Xie, G.-J. Zhang, *Anal. Sci.* **2015**, 31, 73.
- [34] S. Kim, R. Lee, D. Kwon, T.-H. Kim, T. J. Park, S.-J. Choi, H.-S. Mo, D. H. Kim, B.-G. Park, *IEEE Sens. J.* **2021**, 21, 8839.
- [35] D. Park, J. H. Kim, H. J. Kim, D. Lee, D. S. Lee, D. S. Yoon, K. S. Hwang, *Biosens. Bioelectron.* **2020**, 167, 112505.
- [36] J. R. Siqueira, R. M. Maki, F. V. Paulovich, C. F. Werner, A. Poghossian, M. C. F. de Oliveira, V. Zucolotto, O. N. Oliveira, M. J. Schöning, *Anal. Chem.* **2010**, 82, 61.
- [37] Y.-F. Jia, C.-Y. Gao, J. He, D.-F. Feng, K.-L. Xing, M. Wu, Y. Liu, W.-S. Cai, X.-Z. Feng, *Analyst* **2012**, 137, 3806.
- [38] T. Yoshinobu, K.-I. Miyamoto, C. F. Werner, A. Poghossian, T. Wagner, M. J. Schöning, *Annu. Rev. Anal. Chem.* **2017**, 10, 225.
- [39] M. Taing, D. Sweatman, in *11th Electronics Packaging Technology Conf.*, IEEE, Piscataway, NJ **2009**, <https://doi.org/10.1109/EPTC.2009.5416557>.
- [40] M. H. Abouzar, A. Poghossian, A. M. Pedraza, D. Gandhi, S. Ingebrandt, W. Moritz, M. J. Schöning, *Biosens. Bioelectron.* **2011**, 26, 3023.
- [41] S. Dastidar, A. Agarwal, N. Kumar, V. Bal, S. Panda, *IEEE Sens. J.* **2015**, 15, 2039.
- [42] A. Poghossian, R. Welden, V. V. Buniatyan, M. J. Schöning, *Sensors* **2021**, 21, 6161.
- [43] S. Schusser, M. Krischer, M. Bäcker, A. Poghossian, P. Wagner, M. J. Schöning, *Anal. Chem.* **2015**, 87, 6607.
- [44] T. Karschuck, S. Schmidt, S. Achtsnicht, A. Poghossian, P. H. Wagner, M. J. Schöning, in *IEEE International Symposium on Olfaction and Electronic Nose (ISOEN)*, IEEE, Piscataway, NJ **2022**, <https://doi.org/10.1109/isoen54820.2022.9789602>
- [45] D. E. Yates, S. Levine, T. W. Healy, *J. Chem. Soc., Faraday Trans. 1* **1974**, 70, 1807.
- [46] R. van Hal, J. Eijkel, P. Bergveld, *Sens. Actuators, B* **1995**, 24, 201.
- [47] S. Mross, T. Zimmermann, N. Winkin, M. Kraft, H. Vogt, *Sens. Actuators, B* **2016**, 236, 937.
- [48] N. Kumar, A. P. Tiwari, J. Kumar, S. Panda, in *2nd Inter. Symp. on Physics and Technology of Sensors (ISPTS)*, IEEE, Piscataway, NJ **2015**, <https://doi.org/10.1109/ispts.2015.7220115>.
- [49] M. Chen, Y. Jin, X. Qu, Q. Jin, J. Zhao, *Sens. Actuators, B* **2014**, 192, 399.
- [50] A. Poghossian, A. Baade, H. Emons, M. J. Schöning, *Sens. Actuators, B* **2001**, 76, 634.
- [51] C. Kaulen, M. Homberger, S. Bourone, N. Babajani, S. Karthäuser, A. Besmehn, U. Simon, *Langmuir* **2014**, 30, 574.
- [52] J. Polte, *CrystEngComm* **2015**, 17, 6809.
- [53] M. Wuithschick, A. Birnbaum, S. Witte, M. Sztucki, U. Vainio, N. Pinna, K. Rademann, F. Emmerling, R. Kraehnert, J. Polte, *ACS Nano* **2015**, 9, 7052.
- [54] T. S. Bronder, A. Poghossian, M. P. Jessing, M. Keusgen, M. J. Schöning, *Biosens. Bioelectron.* **2019**, 126, 510.
- [55] S. Jamsb, S. Collins, R. L. Smith, *Sens. Actuators, B* **1998**, 49, 146.
- [56] T. S. Bronder, A. Poghossian, S. Scheja, C. Wu, M. Keusgen, D. Mewes, M. J. Schöning, *ACS Appl. Mater. Interfaces* **2015**, 7, 20068.
- [57] T. N. Lee, H. J. H. Chen, Y.-C. Huang, K.-C. Hsieh, *J. Electrochem. Soc.* **2018**, 165, B767.
- [58] F. Dominec, Calculating Size Distribution of Powder Particles Using Image], <https://www.fzu.cz/~dominecf/granulo/index.html> (accessed: October 2021).
- [59] M. J. Schöning, N. Näther, V. Auger, A. Poghossian, M. Koudelka-Hep, *Sens. Actuators, B* **2005**, 108, 986.
- [60] B. Veigas, R. Branquinho, J. V. Pinto, P. J. Wojcik, R. Martins, E. Fortunato, P. V. Baptista, *Biosens. Bioelectron.* **2014**, 52, 50.
- [61] Zahner Elektrik, Thales Remote Python, <https://github.com/Zahner-elektrik/Thales-Remote-Python> (accessed: January 2022).
- [62] M. Klein, *Sens. Actuators, B* **1990**, 1, 354.